analytical chemistry

pubs.acs.org/ac Article

Genetically Encoded Near-Infrared Photocatalysis for Proximity Labeling of Subcellular Proteome

Tianyu Ren,[#] Jinsaibo Gong,[#] Fu Zheng, Jinshan Long, Han Wang, Jianjun He,* Jian-Hui Jiang,* and Peng Zou*

Cite This: *Anal. Chem.* 2025, 97, 14492−14502 Read Online

ACCESS | Metrics & More | Article Recommendations | Supporting Information

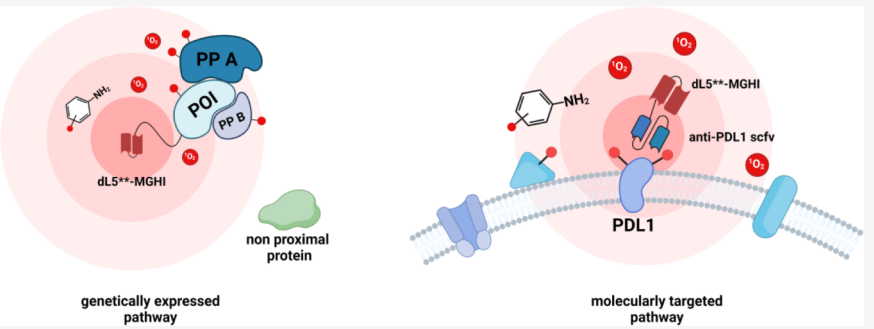

ABSTRACT: The spatial organization of proteins in eukaryotic cells plays essential roles in cellular functions. Genetically encoded proximity labeling methods offer spatially resolved and proteome-wide mapping of protein localization, yet existing techniques are limited to blue light activation, which has limited tissue penetration and causes a high cellular background. Here, we report the development of a near-infrared photocatalytic proximity labeling method, FLAPP, based on the engineered fluorogen-activating protein dL5**. Upon binding to the fluorogenic iodinated malachite green, the complex can efficiently absorb near-IR light to produce singlet oxygen that reacts in situ with nearby histidine residues. Unlike most existing near-infrared light-activated proximity labeling techniques that rely on antibody-dependent membrane targeting, FLAPP is a genetically encoded near-infrared light-activated proximity labeling technology. We demonstrate the high spatial specificity (96%) of FLAPP in the mitochondria and nucleus. FLAPP enables the deep tissue penetration of protein labeling, underscoring its potential for live animal applications.

INTRODUCTION

In eukaryotic cells, the subcellular localization of proteins is intricately linked to their biological functions.[1] For example, mitochondrial proteins involved in energy production and apoptotic signaling must be precisely organized to maintain cellular homeostasis.[2,3] Similarly, enzymes in the endoplasmic reticulum (ER) and Golgi apparatus rely on accurate localization for protein synthesis, modification, and trafficking.[4] Thus, understanding protein function requires detailed knowledge of their spatial arrangements within the native cellular context. While fluorescence microscopy offers high spatial resolution for mapping protein localization, it is often limited by low throughput and the need for prior knowledge of the target protein.[5]

Over the past decade, proximity labeling (PL) has emerged as a powerful tool for unbiased proteome-wide mapping of protein localization. Enzyme-mediated PL employs peroxidases (e.g., APEX2,[6,7] HRP)[8] or biotin ligases (e.g., BioID,[9] TurboID),[10] which are genetically localized to specific subcellular sites via fusion with targeting sequences or protein baits. Upon chemical activation (e.g., hydrogen peroxide for APEX2/HRP or biotin for BioID/TurboID), these enzymes generate short-lived reactive intermediates (e.g., phenoxyl radicals or biotinyl-5′-adenylate) that label proximal proteins. Labeled proteins can then be enriched by affinity purification and identified by mass spectrometry. These techniques have been widely applied to study subcellular proteomes in both cell culture[1,11] and live animals.[12−16] To improve temporal control, photoactivatable PL variants have been developed, including photocaged TurboID (photoTurbo),[17] LOV-Turbo,[18] and SOPP3-APEX2.[19] These systems use mild light illumination rather than chemical additions to trigger the PL reaction, offering 10-min temporal resolution and avoiding cytotoxic reagents such as hydrogen peroxide. However, their reliance on UV or blue light poses challenges due to spectral overlap with endogenous chromophores.[20]

Received: March 26, 2025
Revised: June 18, 2025
Accepted: June 19, 2025
Published: July 1, 2025

Recent advances in photocatalytic PL offer alternative light-triggered approaches. Synthetic photocatalysts, conjugated to antibodies or self-labeling protein tags, enable protein labeling upon visible light activation.[21,22] These methods have been used to profile cell surface proteome[21] and cell−cell interactions.[23] For instance, Tay and coworkers developed a deep red light-activatable photoredox catalyst to label membrane epithelial cell adhesion molecules.[24] Alternatively, organic photosensitizers such as 2-monobromofluorescein can be anchored to a cell surface receptor (e.g., PhoxID)[25] to achieve light-triggered proximity labeling at neuronal synapses in the live mouse brain. However, intracellular applications of synthetic photocatalysts are limited by background signals arising from untargeted catalysts. Protein-based photocatalysts (e.g., CAP-seq,[26] LITag,[27] RinID,[28] PDPL)[29] mitigate this issue by enabling genetic targeting but are restricted to blue light activation, which can cause background labeling due to endogenous photosensitizers like flavoproteins.[20] Photocatalysis under near-infrared (NIR) illumination could effectively reduce this background. For example, NIR light-activated photosensitizers have been conjugated to antibodies to achieve PL on the cell surface or premetallized cells.[22,24,30] Alternatively, they can be conjugated to small molecules to target specific protein baits or organelles.[31−33] However, antibodies are not readily targetable to intracellular protein baits in live cells, and small molecule-based directing approaches often suffer from background signals arising from untargeted photocatalysts.[26] A genetically encoded photocatalytic protein PL method activated by NIR light with minimal background is still lacking.

Genetically encoded self-labeling protein tags have been employed to covalently (e.g., HaloTag)[34,35] or noncovalently (e.g., FAST)[36] anchor small molecule chromophores. Fluorogen-activating proteins (FAPs) are engineered to bind and activate fluorogens for fluorescence or singlet oxygen ($^1O_2$) production upon light illumination.[37] The FAP protein tag dL5**, originally developed for fluorescence imaging applications, features high fluorogenicity upon binding to malachite green (MG) derivatives and enables visualization of fused proteins with low background.[38] He and coworkers introduced a di-iodinated MG variant (MG2I) that generates $^1O_2$ under near-infrared (NIR) light for protein inactivation and cell ablation in live tissue.[37] This technique has been extended to the oxidative damage of DNA, mitochondrial inactivation, and functional cell ablation *in vivo*. More recently, Li and coworkers demonstrated that monoiodide MG derivatives (MGHI) outperform MG2I in RNA labeling, as their reduced decay rates preserve fluorescence emission and intersystem crossing.[39] However, the protein labeling capability of dL5** has not been investigated.

Herein, we present FLAPP (fluorogen-activating protein-mediated photocatalytic proximity labeling), a method that utilizes cell-permeable fluorogens and photocatalysis for efficient and spatially resolved protein labeling. FLAPP exploits iodinated fluorogens bound to a fluorescence-activating protein, enabling protein labeling under NIR light (Scheme 1). We systematically investigated the FLAPP mechanism and demonstrated its broad applicability for protein labeling across multiple subcellular compartments.

Scheme 1. Schematic Illustration of dL5-MGHI for Proximity Protein Labeling under Near-Infrared Light Irradiation**

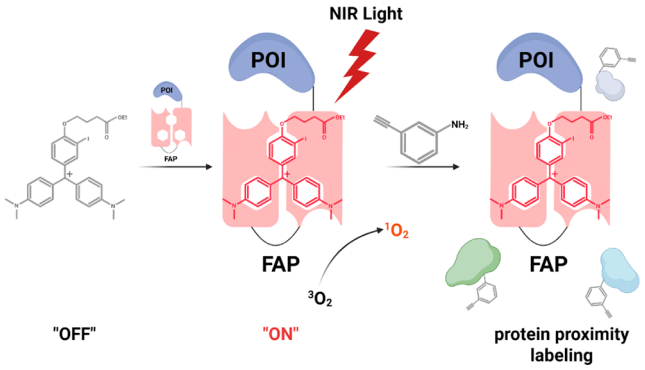

EXPERIMENTAL SECTION

Synthesis of MG Derivatives. The synthetic steps for MG derivatives are described in detail in the Supporting Information.

Western Blot Analysis of FLAPP Labeling of BSA *In Vitro*. For proximity labeling assay *in vitro*, 10 μM purified dL5**, 10 μM MG-ester (MGHI or MG2I), 100 μM biotin-aniline or biotin-phenol, and 0.1 mg/mL bovine serum albumin (BSA) were mixed in phosphate-buffered saline (PBS) in a 100 μL total reaction volume. The reaction mixture was irradiated with 660 nm LED light for 2 min at room temperature. For labeling through tissue of various thicknesses, 10 μM purified dL5**, 10 μM MGHI or Hypocrellin A, 100 μM biotin-aniline, and 0.1 mg/mL BSA were mixed in PBS in a 100 μL total reaction volume. Pork slices with varying thicknesses (1 mm, 2 mm, 3 mm, 4 mm, or 5 mm) were inserted between the reaction mixture and the light source. The reaction mixture was illuminated under 450 nm light (for Hypocrellin A) or 660 nm light (for MGHI) at room temperature for 2 min. After irradiation, 4x loading buffer was added directly to the mixture, and the samples were boiled for 10 min at 95 °C. The samples were analyzed by streptavidin-HRP Western blot.

Fluorescence Imaging of FLAPP Labeling in Living Cells. Cells were seeded in confocal dishes at a density of ∼20,000 cells. After 24 h, cells were washed once with PBS, incubated with 1 mM 3EA and 500 nM MGHI in fresh Hanks' Balanced Salt Solution for 1 h at 37 °C, and then illuminated with a red LED (660 nm) for 10 min at room temperature. Thereafter, cells were washed twice with PBS and fixed with 4% formaldehyde in PBS at room temperature for 15 min. Excess formaldehyde was removed from the fixed cells by washing three times with PBS. Cells were then permeabilized with 0.5% Triton X-100 in PBS and subsequently washed three more times with PBS. Next, 100 μL mixture of click reaction reagents was added to each sample, containing 50 μM Cy3-azide, 2 mM $CuSO_4$, 1 mM BTTAA and 0.5 mg/mL sodium ascorbate, and incubated at room temperature for 30 min (or click reagent containing 100 μM N_3-biotin, 667 μM $CuSO_4$, 1.3 mM BTTAA, and 2.5 mM sodium ascorbate, followed by staining with streptavidin-AlexaFlour568). After the click reaction, cells were washed six times with PBS containing 0.05% Tween-20 (PBST) and then blocked with 5% BSA in PBST for 30 min at room temperature. For immunostaining to enable colocalization analysis, cells were incubated with

https://doi.org/10.1021/acs.analchem.5c01826
Anal. Chem. 2025, 97, 14492−14502

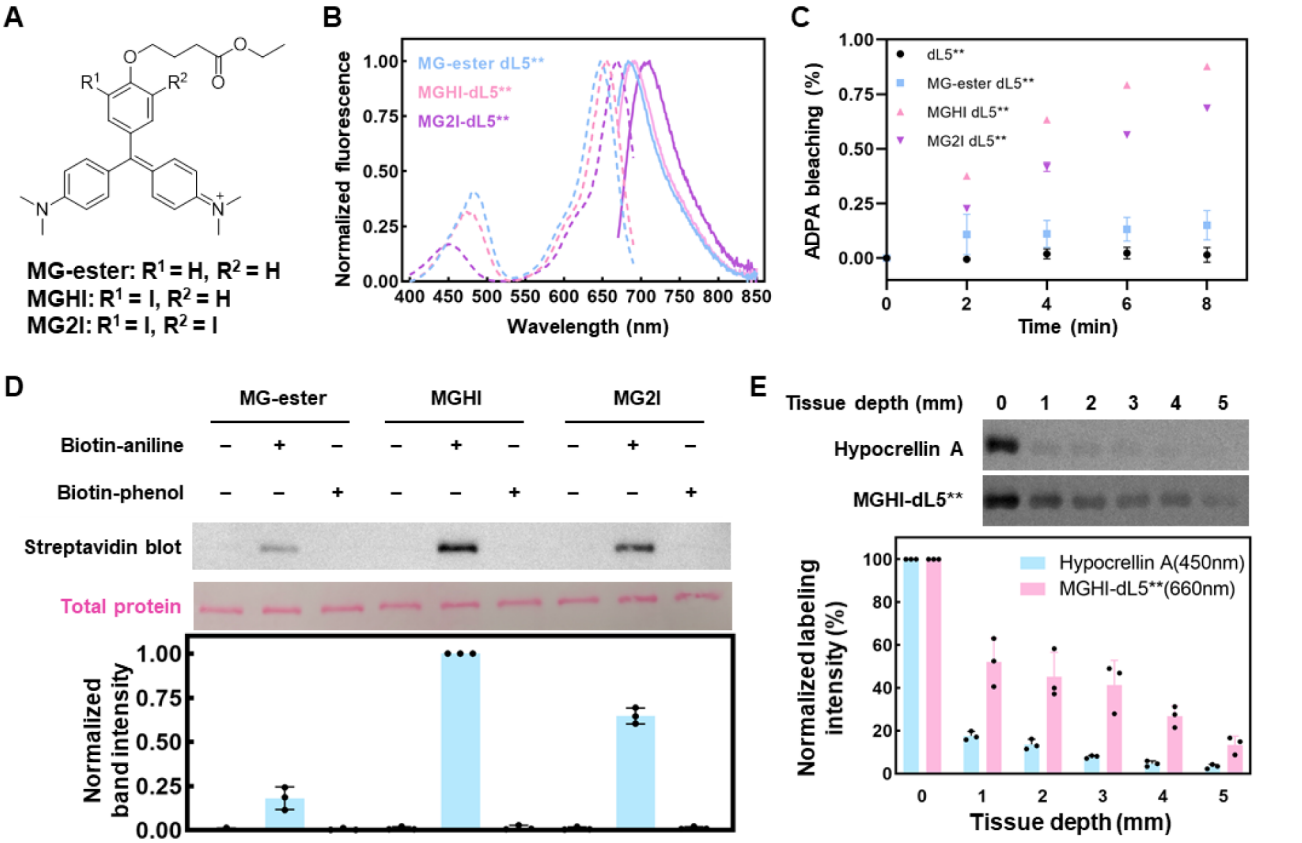

Figure 1. *In vitro* Characterizations of ROS generation and protein labeling capability by FLAPP. (A) Structure of MG-ester, MGHI, MG2I. (B) Normalized excitation (dashed lines) and emission (solid lines) spectra of MG-ester, MGHI, MG2I binding to dL5**, with 1 μM of fluorogen complexed with 1 μM dL5**. The fluorescence intensity was normalized to the peak. (C) Generation of $^1O_2$ by dL5** complexed with MG-ester, MGHI, and MG2I, assessed on the basis of ADPA bleaching. Fluorescence bleaching was monitored at 374 nm excitation wavelength and 402 nm emission wavelength over varying durations of 660 nm light exposure. (D) Comparison of different probes for photolabeling of bovine serum albumin (BSA), with 2 min light exposure. (E) Streptavidin blot analysis of BSA labeled with dL5**-MGHI (at 660 nm) and Hypocrellin A (at 450 nm) through tissue with varying thicknesses.

primary antibody (mouse anti-V5 or anti-HA antibody at 1:1000 dilution, and rabbit antibody for organelle markers at the recommended dilution ratio) overnight at 4 °C. After washing three times with PBST, cells were incubated with secondary antibody (goat antimouse AlexaFluor488/647, streptavidin-AlexaFlour568/647 at 1:1000 dilution) for 2 h at room temperature. Cells were then washed three times with PBST and counterstained with Hoechst 33258 (or DAPI) solution in PBS for 10 min at room temperature. Immunofluorescence images were collected using a ZEISS LSM 980 confocal microscope.

RESULTS AND DISCUSSION

We began by synthesizing the MG-ester fluorogen and its mono- and di-iodinated derivatives, MGHI and MG2I, respectively (Figure 1A). The iodinated fluorogens exhibited red-shifted absorption and emission spectra upon binding to the dL5** protein, a shift attributed to the heavy atom effect[37] (Figure 1B). To evaluate their capability to generate $^1O_2$, we monitored the photobleaching of anthracene-9,10-dipropionic acid (ADPA). While MG-ester showed negligible singlet oxygen yield, MGHI and MG2I effectively generated $^1O_2$, with MGHI exhibiting superior efficiency compared to MG2I (Figure 1C).

Next, we assessed the potential of dL5**-fluorogen complexes to label proteins *in vitro* using biotin-aniline (BA) and biotin-phenol (BP) as probes. We chose bovine serum albumin (BSA) as a model and mixed the protein with dL5**, fluorogens (MG, MGHI, or MG2I), and the biotin-conjugated probes, followed by 660 nm LED illumination at 28 W/cm^2 for 2 min. For all three fluorogens, immunoblotting with HRP-conjugated streptavidin revealed the robust biotinylation of BSA in the presence of 100 μM BA (Figure 1D). Notably, little labeling was observed for proteins incubated with the BP probe, indicating that the photoreaction did not involve the generation of phenoxyl free radicals. The labeling intensities of dL5**-MGHI and dL5**-MG2I complexes increased with illumination time (Figure S1), with MGHI exhibiting stronger labeling efficiency than MG2I (Figure 1D), which we attributed to the higher singlet oxygen yield of dL5**-MGHI.[40]

The 660 nm NIR light used for activating dL5**-MGHI could penetrate deeper into biological tissues than blue light due to reduced scattering and lower absorption by water and hemoglobin.[41] To quantitatively measure the tissue penetration of NIR photocatalysis, we placed pork slices of varying thicknesses between the 660 nm LED light source and the dL5**-MGHI reaction solution (Figure S2). As the pork slice thickness increased from 0 to 4 mm, dL5**-MGHI labeling gradually decreased but still retained approximately 30% of its labeling efficacy even at 4 mm tissue thickness, which is consistent with the previous report that NIR light penetrates to

https://doi.org/10.1021/acs.analchem.5c01826
Anal. Chem. 2025, 97, 14492−14502

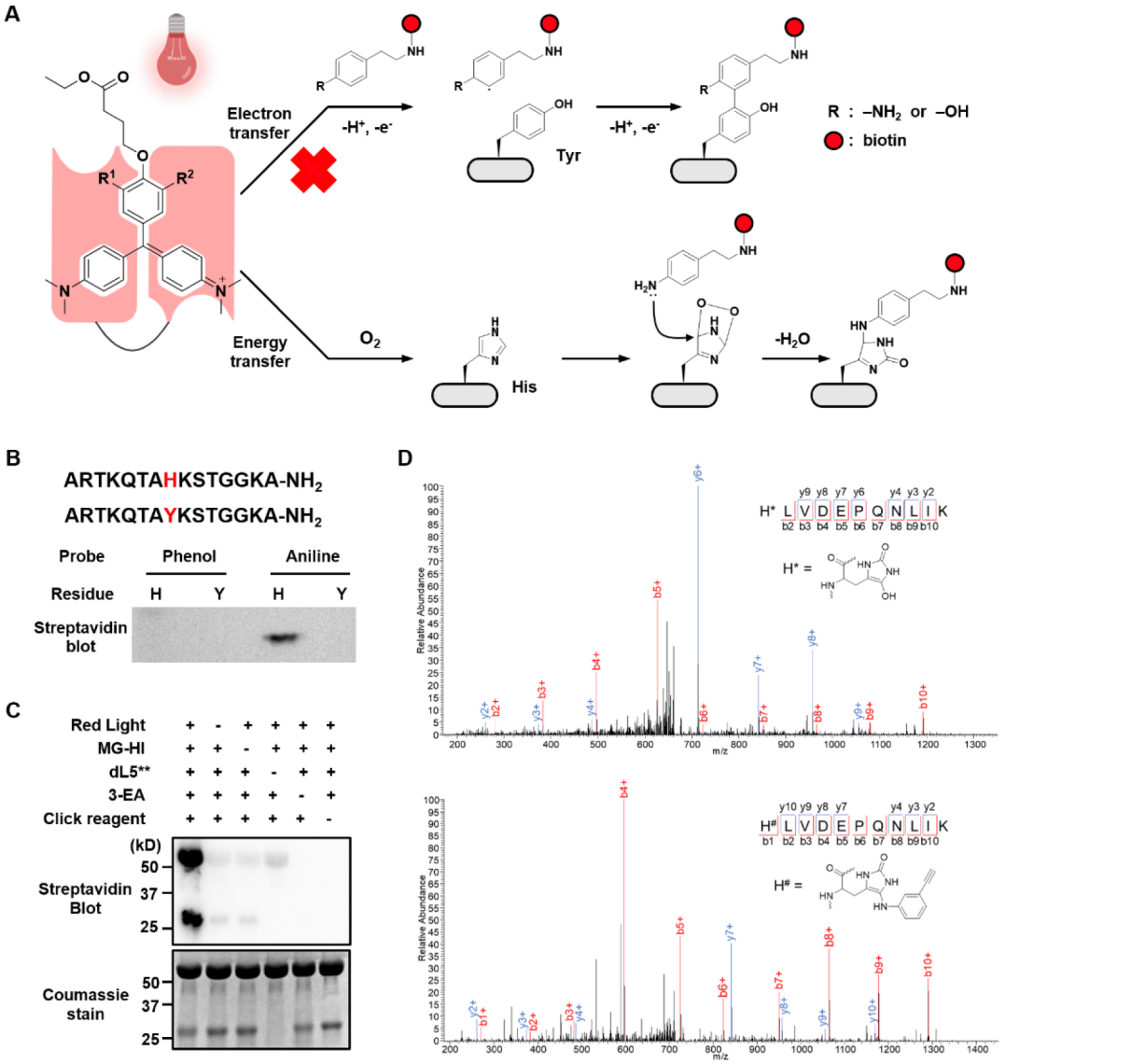

Figure 2. Mechanism of FLAPP-mediated photocatalytic proximity labeling. (A) Proposed mechanisms and predicted amino acid reaction sites involved in FLAPP-mediated proximity labeling. (B) Western blot analysis of 15-mer peptides containing a single active residue (Y or H) labeled by FLAPP. Peptides (1 mg/mL) were dissolved in phosphate buffered saline (PBS) in the presence of 100 μM BP or BA, 10 μM MGHI, and 10 μM dL5**, followed by 2 min of irradiation. (C) Western blot and SDS-PAGE analysis of MGHI–dL5** mediated photoproximity labeling of bovine serum albumin (BSA). (D) MS/MS spectra of a representative peptide with histidine residue oxidized to 5-hydroxy-1,5-dihydro-2-oxoimidazole (top) and 5-(3-ethynylphenyl)amino-1,5-dihydro-2-oxoimidazole (bottom).

a depth of 3–4 mm into tissue[22] (Figure 1E). For comparison, we performed photocatalytic labeling mediated by Hypocrellin A, which is activated by 450 nm blue LED light.[42] As expected, Hypocrellin A exhibited a sharp decrease in labeling intensity in the presence of a pork slice, with less than 5% labeling intensity remaining at 4 mm tissue depth. This comparison underscores the advantages of NIR light for protein labeling in tissue environments.

We next investigated the photo-oxidation mechanism of FLAPP. Photo-oxidation typically proceeds via two nonexclusive pathways: (1) single-electron transfer (SET), in which the photocatalyst converts phenol into phenoxy free radicals to label tyrosine residues, and (2) energy transfer, where the photocatalyst activates molecular oxygen into singlet oxygen to react with histidine residues, leading to the formation of an endoperoxide intermediate (Figure 2A). To distinguish between these two mechanisms, we prepared two 15-mer peptides (ARTKQTAYKSTGGKA and ARTKQTAHKSTGGKA) whose sequences differ by only one amino acid residue in the middle: tyrosine versus histidine. Consistent with the BSA labeling experiment, no biotinylation was detected for either peptide when BP was used as the probe (Figure 2B). Using BA as the probe, we observed strong biotinylation with the histidine-containing peptide following FLAPP labeling but negligible biotinylation with the tyrosine-containing peptide. Mass spectrometry analysis further confirmed the presence of biotin-aniline modification on the histidine residue (Figure S3).

To further confirm the FLAPP labeling mechanism on protein samples, we mixed BSA, dL5**, and MGHI with another aniline probe, 3-ethynylaniline (3-EA). Following red light illumination for 20 min, the protein sample was reacted with biotin-conjugated azide via copper-assisted alkyne–azide cycloaddition (CuAAC) reaction. Strong biotinylation of BSA

https://doi.org/10.1021/acs.analchem.5c01826
Anal. Chem. 2025, 97, 14492–14502

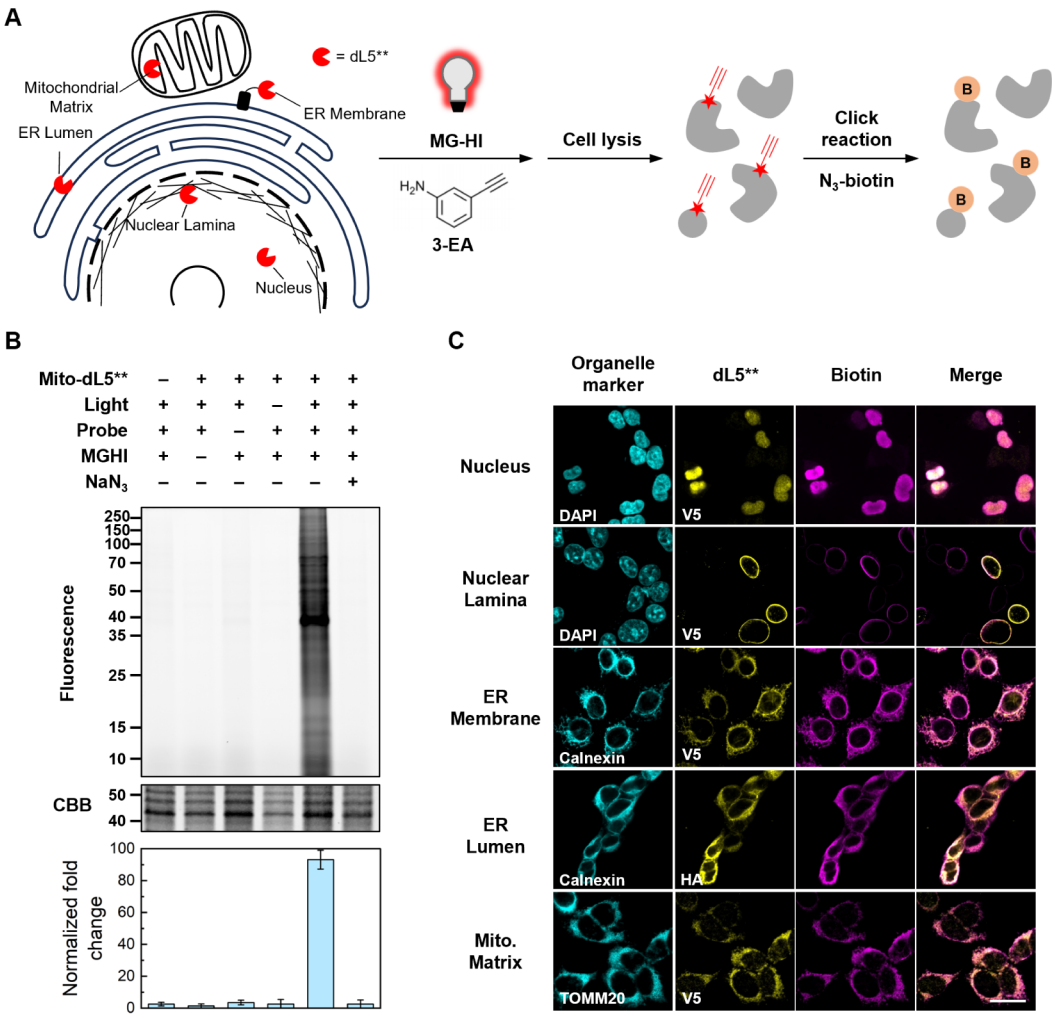

Figure 3. Application of FLAPP at different subcellular localizations in living cells. (A) Schematic illustration of the FLAPP workflow with dL5** targeted to various subcellular locations. (B) In-gel fluorescence analysis comparing FLAPP labeling in MCF-7 cells expressing mito-dL5** with control experiments that omitted dL5**, red light illumination, probe (3-EA), and MGHI. Another control sample contains sodium azide. Quantitation of fluorescence data is shown at the bottom, normalized by Coomassie brilliant blue signal. Data represent the average of 3 replications. (C) Confocal fluorescence images of HEK293T cells labeled with FLAPP in various organelles. Scale bar: 10 μm. dL5** was fused to V5 or HA tags.

was detected on a streptavidin blot, while minimal background signal was observed in the absence of light, MGHI, dL5**, or 3-EA (Figure 2C). We proceeded to digest the photolabeled BSA with trypsin and analyzed the peptides using liquid chromatography-tandem mass spectrometry (LC-MS/MS). As expected, histidine modifications, including conversion of the imidazole ring into oxidative intermediates (+31.9898 Da) and conjugation products with 3-EA (+131.0371 Da), were detected (Figure 2D). We also searched for potential oxidative modifications by 3-EA on tyrosine, tryptophan, cysteine, and methionine residues. Interestingly, a previously unreported cysteine adduct (+131.0371 Da) was identified, with a mass shift consistent with the formation of a sulfinamide-like structure (Figure S4). Formation of these oxidative conjugation products is dependent on NIR light illumination. For the other amino acid residues, our search did not reveal light-dependent modifications under our experimental conditions (30 W/cm^2 NIR light for 20 min in the presence of 1 mM 3-EA).

To investigate the FLAPP labeling mechanism, we repeated the photocatalytic reactions in the presence of reactive oxygen species (ROS) and free radical quenchers. Notably, protein labeling was significantly suppressed in the presence of sodium azide, a compound recognized for its ability to quench singlet oxygen. Conversely, when the reaction was carried out in 80% v/v D_2O, which stabilizes singlet oxygen, the labeling signal intensity was slightly enhanced by approximately 15% (Figure S5). To further explore the potential role of additional reactive oxygen species, mannitol (a hydroxyl radical scavenger) and vitamin C (a superoxide radical inhibitor) were introduced into the reaction. However, neither agent showed a measurable effect on labeling efficiency under the experimental conditions. Collectively, these findings indicate that singlet oxygen, rather than hydroxyl or superoxide radicals, plays the predominant role in mediating the labeling process.

To evaluate the efficiency of FLAPP labeling in live cells, we established MCF-7 (Michigan Cancer Foundation-7) cell lines stably expressing dL5** targeted to the nucleus (H2B-dL5**, via fusion with the histone protein H2B) and mitochondria (mito-dL5**, via N-terminal fusion with the 23-amino-acid mitochondrial targeting sequence derived from cytochrome c oxidase subunit COX4.[29] Confocal imaging of MG-ester

https://doi.org/10.1021/acs.analchem.5c01826
Anal. Chem. 2025, 97, 14492−14502

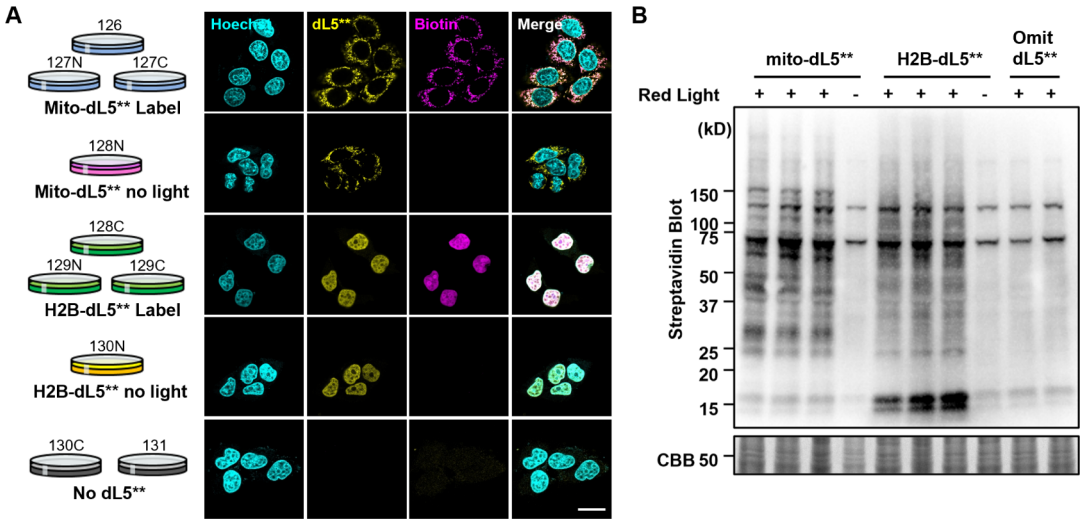

Figure 4. Scheme of mitochondrial and nuclear proteomes identified by FLAPP. (A) Scheme of TMT10-based proteome identification and confocal images corresponding to each experimental condition. Scale bar: 10 μm. (B) Western blot analysis of TMT10 samples from (A).

fluorescence confirmed accurate subcellular localization (Figure S6). Flow cytometry further demonstrated high expression levels of dL5** in both cell lines (Figure S7). To assess FLAPP's singlet oxygen generation in cells, we incubated MCF-7 H2B-dL5** cells with MGHI and the ROS probe DCFH-DA.[43] Following NIR light illumination, the resulting ROS oxidizes intracellular DCFH to yield a green fluorescence (Figure S8). No green fluorescence was observed in the absence of MGHI or light, or in cells not expressing dL5**. When cells were treated with the singlet oxygen scavenger sodium azide,[29] green fluorescence from the ROS probe was abolished (Figure S8).

We next optimized the experimental conditions for the FLAPP labeling of cellular proteins. MCF-7 cells expressing mito-dL5** were treated with MGHI and 3-EA at various concentrations, followed by 660 nm red light illumination (Figure 3A). Cells were then lysed, and the proteins in the lysate were reacted with TAMRA-conjugated azide via a CuAAC reaction. In-gel fluorescence analysis revealed sufficient labeling signals with 1 mM 3-EA, 500 nM MGHI, and 10-min illumination, which were used for subsequent experiments (Figure S9). A strong protein biotinylation signal was observed in mito-dL5** samples but not in the wild-type cells or in the absence of MGHI or light (Figure 3B). Consistent with data from *in vitro* assays, we observed minimal labeling in the presence of sodium azide.

To evaluate the spatial specificity of FLAPP labeling in cells, we generated HEK293T cell lines expressing dL5** targeted to various organelles, including the nucleus, nuclear lamina, ER membrane, ER lumen, and mitochondrial matrix. After the cells were illuminated with NIR light in the presence of 500 nM MGHI and 1 mM 3-EA, the samples were fixed and stained with antibodies against organelle-specific markers. Labeled proteins were visualized via a CuAAC reaction with biotin-conjugated azide, followed by staining with streptavidin-conjugated fluorophores. Confocal fluorescence imaging revealed excellent colocalization of FLAPP-labeled proteins with dL5** expression and organelle markers, confirming the high spatial specificity of FLAPP in live cells (Figure 3C).

We further validated the general applicability of FLAPP in A549 and HeLa cells expressing H2B-dL5** and Mito-dL5**, respectively. Consistent with expectations, fluorescence signals originating from distinct subcellular organelles were clearly observed, accompanied by good colocalization with the tagged proteins (Figure S10). To demonstrate the tissue penetration capability of FLAPP, we illuminated MCF-7 cells expressing H2B-dL5** with NIR light through tissue of varying thicknesses. As expected, while the labeling intensity was attenuated gradually with increasing tissue thickness, nearly 25% of the labeling signal remained even at a tissue thickness of 4 mm (Figure S11). Together, these results demonstrate the versatility of FLAPP for precise labeling of subcellular proteins.

To demonstrate the broad applicability of FLAPP in labeling cellular proteins, we extended FLAPP to target cell surface proteins proximal to a specific membrane protein bait. Using the SpyTag-SpyCatcher system, we covalently conjugated a dL5** to an anti-PDL1 single-chain variable fragment (scFv) (Figure S12). Incubation of the resulting anti-PDL1-dL5** conjugate with MDA-MB-231 breast cancer cells expressing PDL1 produced a strong far-red fluorescence signal on the cell surface (Figure S12). In contrast, minimal fluorescence was observed when the conjugate was incubated with HEK293 cells lacking PDL1 expression, confirming the conjugate's specificity for cell surface PDL1. Upon NIR illumination, MDA-MB-231 cells treated with anti-PDL1-dL5**, MGHI, and BA exhibited robust membrane-specific labeling. Control samples lacking fluorogen, dL5**, or light showed significantly reduced labeling, as confirmed by fluorescence microscopy and flow cytometry (Figure S12).

We evaluated the spatial specificity and proteomic coverage of FLAPP labeling in live cells using quantitative mass spectrometry. Two MCF-7 cell lines were analyzed: MCF-7 mito-dL5** and MCF-7 H2B-dL5**, which targets dL5** to the mitochondrial matrix and nucleus, respectively. Quantitative proteomics was performed using TMT10-plex isotope tagging (Figure 4A). Negative controls, which omitted either red light illumination or dL5** expression, were included to minimize background labeling. Confocal immunofluorescence imaging confirmed that FLAPP labeling precisely colocalized with dL5** expression in both cell lines.

In the proteomic labeling experiments, MCF-7 cells were treated with 500 μM MGHI and 1 mM 3-EA, then illuminated with 660 nm red light before lysis. The lysates were reacted via CuAAC with a biotin-conjugated azide, and biotinylated

https://doi.org/10.1021/acs.analchem.5c01826
Anal. Chem. 2025, 97, 14492−14502

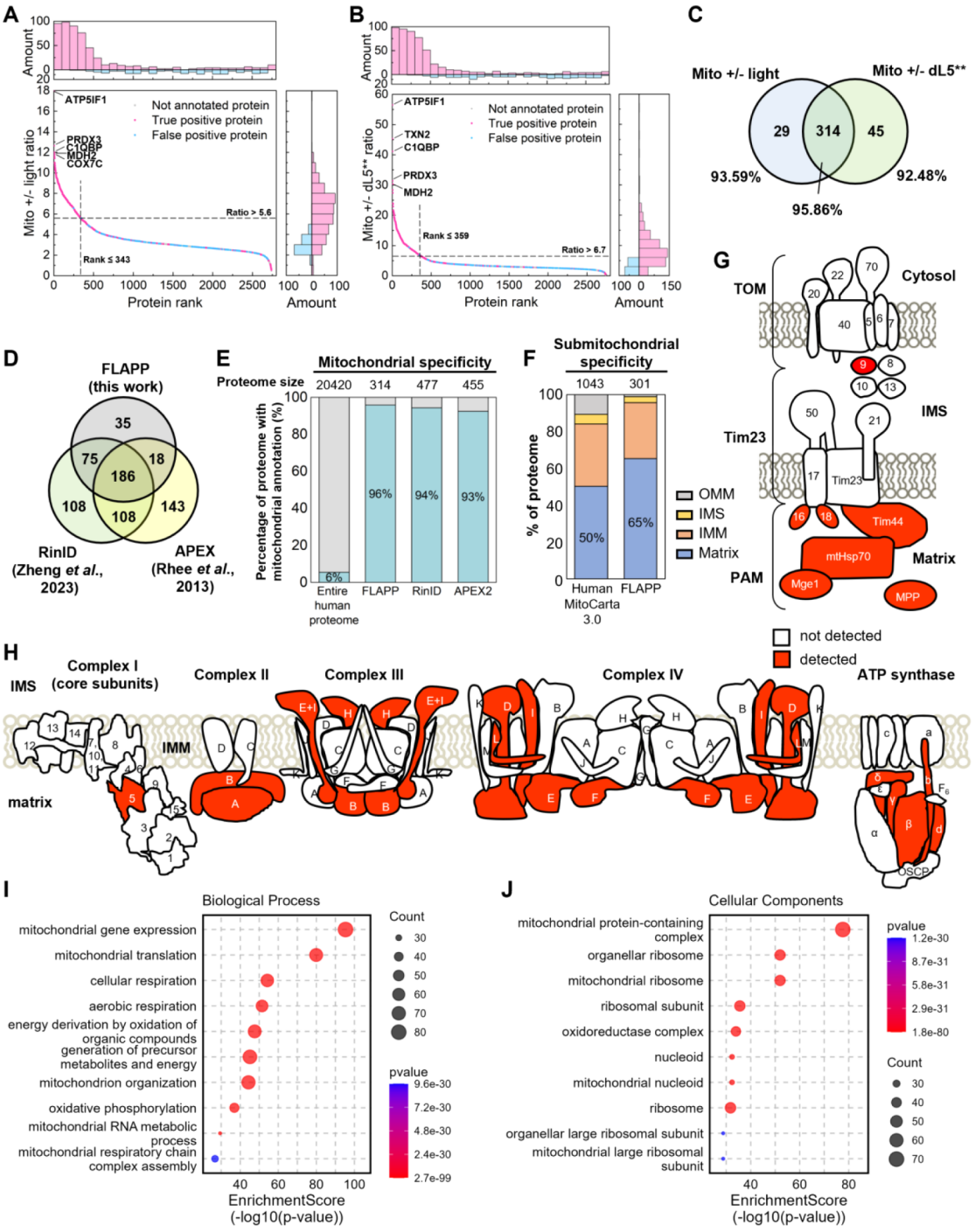

Figure 5. Analysis of mitochondrial proteomes identified by FLAPP. (A-B) FLAPP-labeled mitochondrial proteins ranked by the ratio between samples with and without red light illumination (A) or dL5** expression (B). Histograms showing the number of true-positive (pink) and false-positive (blue) proteins are shown at the top and right. (C) Intersection between "mito ± light" and "mito ± dL5**" data sets. (D,E) Comparisons of the coverage (D) and spatial specificity (E) of FLAPP mitochondrial proteomic data with RinID and APEX. (F) Submitochondrial specificity analysis of FLAPP mitochondrial matrix proteome. (G,H) Cartoon representation of FLAPP protein coverage in the TOM/TIM/PAM protein-import machinery (G) and the electron transport chain complexes (H) embedded in the mitochondrial inner membrane. (I,J) Gene Ontology Biological Processes (GOBP, I) and Cellular Component (GOCC, J) analyses of FLAPP mitochondrial matrix proteome.

proteins were enriched using streptavidin-coated agarose beads. The success of both the labeling and enrichment steps was verified by SDS-PAGE (Figure 4B) and silver staining (Figure S13). The enriched proteins were digested with trypsin, isobarically labeled with TMT reagents, and analyzed by quantitative LC-MS/MS. To ensure consistency across samples, TMT reporter ion intensities were normalized to the endogenous biotinylated protein pyruvate carboxylase. High reproducibility was observed among replicates, with Pearson's correlation coefficients exceeding 0.98 (Figure S14).

For the mitochondrial proteome, we calculated an enrichment ratio ("mito ± light") for each protein by dividing its average TMT reporter ion intensity from three mito-dL5** replicates (channels 126, 127N, and 127C) by its intensity

https://doi.org/10.1021/acs.analchem.5c01826
Anal. Chem. 2025, 97, 14492−14502

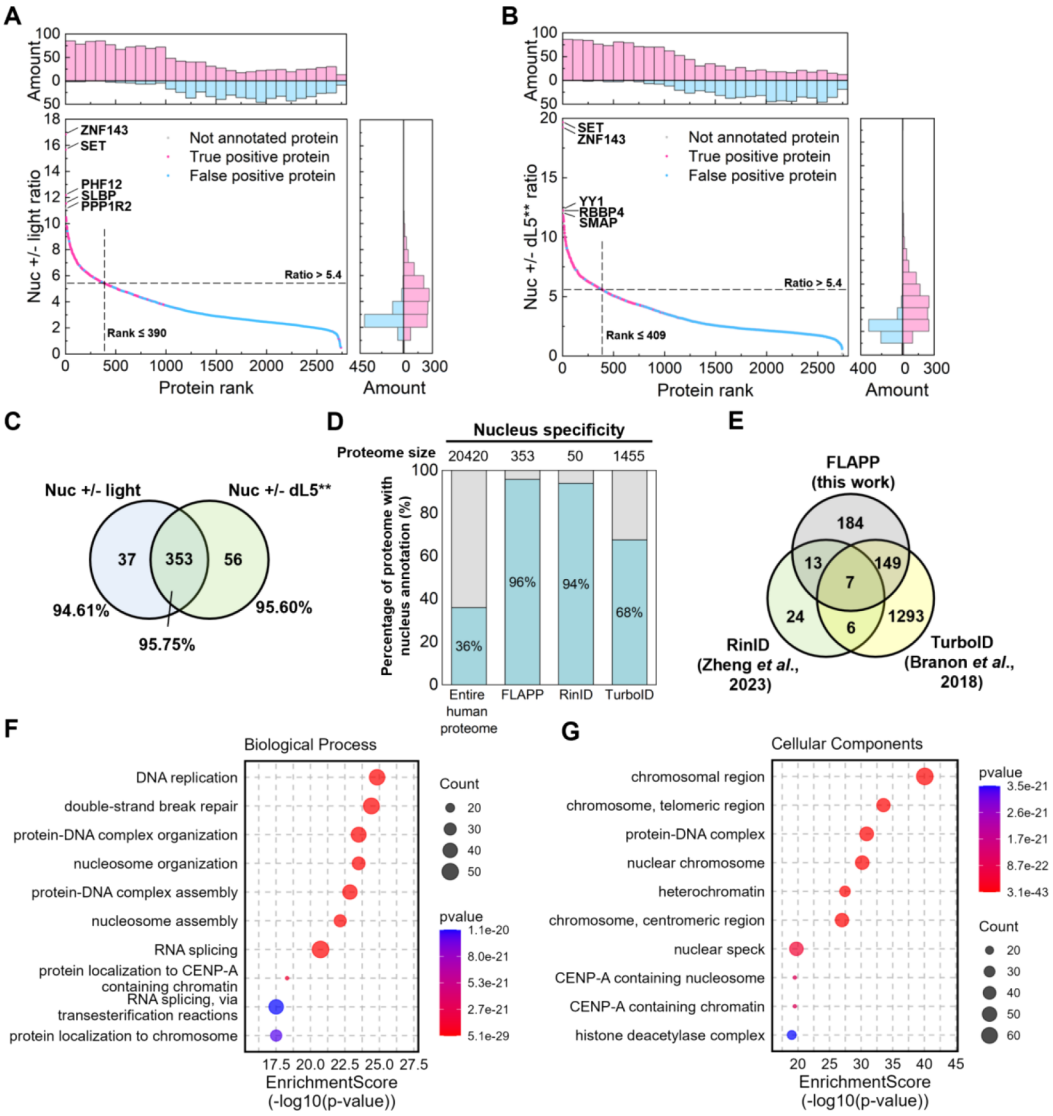

Figure 6. Analysis of Nuclear Proteomes Identified by FLAPP. (A-B) FLAPP-labeled nuclear proteins ranked by the ratio between samples with and without red light illumination (A) or dL5** expression (B). Histograms showing the number of true-positive (pink) and false-positive (blue) proteins are shown at the top and right. (C) Intersection between "nuc ± light" and "nuc ± dL5**" data sets. (D-E) Comparisons of the spatial specificity (D) and coverage (E) of FLAPP nuclear proteomic data with RinID and TurboID. (F-G) GOBP and GOCC analysis of identified nuclear proteome.

from a negative control lacking red light (channel 128N) (Table S1). Proteins were ranked by this "mito ± light" ratio (Figure 5A). To determine the cutoff ratio, we compiled a "true positive" list from MitoCarta 3.0, which is a curated database of mitochondrial proteins.[44] Similarly, a "false-positive" list was defined from proteins previously annotated as false positives in TurboID studies[10] (Table S2). Most of the top-ranked proteins belonged to the true positive list, with false positives ranking low (Figure 5A). For instance, the top ten proteins include tricarboxylic acid (TCA) cycle enzymes such as citrate synthase and malate dehydrogenase, ATPase inhibitor ATPIF1, mitochondrial transcription factor TFAM, mitochondrial ribosomal protein MRPL12, mitochondrial thioredoxin TXN2, thioredoxin-dependent peroxide reductase PRDX3, etc. (Table S1). Using a cutoff ratio of 5.6, we identified 343 enriched proteins in the "mito ± light" data set.

A parallel analysis was performed using negative controls omitting dL5** expression. Here, the "mito ± dL5**" ratio was calculated for each protein by comparing its average intensity from three mito-dL5** replicates (channels 126, 127N, and 127C) with that from negative controls (channels 130C, 131) (Table S1). Again, true positive proteins were enriched at the top of the ranked list (Figure 5B), and a cutoff ratio of 6.7 identified 359 enriched proteins. The intersection of the "mito ± light" and "mito ± dL5**" data sets contained 314 proteins, which we defined as the mitochondrial proteome (Figure 5C and Table S1).

FLAPP's mitochondrial proteome demonstrated exceptional specificity, with 96% (301 out of 314) of proteins matching the predictions from MitoCarta 3.0. This level of specificity surpassed that of APEX (92%) and RinID (94%) in the same subcellular compartment (Figure 5E). FLAPP's mitochondrial coverage (314 proteins) was comparable to that of RinID (477 proteins) and APEX (495 proteins), with 186 overlapping proteins (Figure 5D). The similarity between FLAPP and RinID data sets likely reflects their shared histidine-targeting mechanisms, whereas APEX targets tyrosine residues.

https://doi.org/10.1021/acs.analchem.5c01826
Anal. Chem. 2025, 97, 14492−14502

In terms of submitochondrial specificity, 65% and 30% of the identified mitochondrial proteome were mitochondrial matrix and inner membrane proteins, respectively (Figure 5F and Table S4). To further examine the coverage and the spatial specificity of FLAPP, we mapped the proteomic data set onto TOM/TIM/PAM protein import pathway complexes (Figure 5G) and the electron transport chain complexes (Figure 5H). Our analysis revealed that most proteins identified in these complexes are exposed to the mitochondrial matrix. Gene Ontology Biological Process (GOBP, Figure 5I) and Cellular Components (GOCC, Figure 5J) analyses revealed that the identified proteome exhibited strong compositional and functional associations with mitochondria, demonstrating the high specificity of the data set.

We employed a similar strategy to define the nuclear proteome. For each protein, a "Nuc ± light" ratio was calculated by dividing the average TMT reporter ion intensity from three H2B-dL5** replicates (channels 128C, 129N, and 129C) by that from the no-light control (channel 130N) (Figure 6A and Table S1). Based on previous TurboID studies,[10] proteins associated with the nucleoplasm and nucleolus were designated as true positives, while mitochondrial and extracellular proteins were considered false positives (Table S3). A cutoff ratio of 5.4 yielded 390 enriched proteins in the "Nuc ± light" data set. Similarly, analysis of the negative control omitting dL5** expression produced 409 enriched proteins at the same cutoff (Figure 6B). The overlap between these data sets resulted in 353 proteins, which we defined as the nuclear proteome (Figure 6C and Table S1).

FLAPP demonstrated remarkable nuclear specificity, with 96% (338 out of 353) of the proteins matching the true positive list, surpassing RinID (94%) and TurboID (68%) (Figure 6D and Table S1). Additionally, FLAPP achieved substantially greater coverage, identifying 353 proteins compared to RinID's 50 proteins (Figure 6E). GOBP (Figure 6F) and GOCC (Figure 6G) analyses revealed that the identified proteome was associated with DNA-related biological processes, suggesting that the observed biotinylation may preferentially occur on proteins interacting with histone H2B. Notably, among the top five proteins in both the "Nuc ± light" and "Nuc ± dL5**" data sets, two proteins (protein phosphatase inhibitor 2 and C11orf58) had not been previously annotated as nuclear. Examination of the Human Protein Atlas[45] confirmed nucleoplasmic localization for both proteins, although protein phosphatase inhibitor 2 (PPP1R2) also showed cytoplasmic signals, and C11orf58 displayed ER lumen localization. These observations suggest that the nuclear roles of these proteins merit further investigation.

CONCLUSION

In summary, we have developed FLAPP, an NIR photocatalytic PL method for spatially resolved proteomic profiling in live cells. FLAPP is broadly applicable across various cell lines and subcellular compartments, with its photocatalytic reaction controllable using a commercially available LED at modest illumination intensity. Notably, FLAPP demonstrates exceptional specificity and coverage in the mitochondrial matrix and nucleus, surpassing established proximity labeling methods such as APEX[26] and RinID.[28] These results establish FLAPP as a versatile tool for spatially resolved protein profiling.

FLAPP leverages fluorogen-activating protein dL5** to genetically target iodinated malachite green derivatives to specific subcellular compartments. Unlike other self-labeling protein tags, such as HaloTag,[34,35] the malachite green dye in FLAPP remains minimally photocatalytic until bound to dL5**. This turn-on feature significantly reduces background labeling from untargeted dyes, thereby ensuring high signal specificity.

Another key advantage of FLAPP is its activation by a long-wavelength light source (660 nm LED). Compared to blue light-induced PL methods such as RinID,[28] LITag,[27] and PDPL,[29] the longer wavelength avoids activating endogenous cellular photosensitizers such as flavoproteins. Moreover, NIR activation allows deeper tissue penetration, as demonstrated in this study, where the 660 nm LED effectively drove the photocatalytic reaction through a 4 mm tissue slice. This capability positions FLAPP as a promising tool for tissue-specific PL in future applications.

ASSOCIATED CONTENT

Supporting Information

The Supporting Information is available free of charge at https://pubs.acs.org/doi/10.1021/acs.analchem.5c01826.

Table S1. Mitochondrial and nuclear proteomic datasets (XLSX)

Table S2. List of true positive and false positive mitochondrial proteins (XLSX)

Table S3. List of true positive and false positive nuclear proteins (XLSX)

Table S4. List of sub-mitochondrial proteins (XLSX)

Experimental section, supplementary figures (PDF)

AUTHOR INFORMATION

Corresponding Authors

Jianjun He − *State Key Laboratory of Chemo/Biosensing and Chemometrics, College of Chemistry and Chemical Engineering, Hunan University, Changsha 410082, China;* orcid.org/0000-0001-9779-2662; Email: jianjunh@hnu.edu.cn

Jian-Hui Jiang − *State Key Laboratory of Chemo/Biosensing and Chemometrics, College of Chemistry and Chemical Engineering, Hunan University, Changsha 410082, China;* orcid.org/0000-0003-1594-4023; Email: jianhuijiang@hnu.edu.cn

Peng Zou − *College of Chemistry and Molecular Engineering, Synthetic and Functional Biomolecules Center, Beijing National Laboratory for Molecular Sciences, Key Laboratory of Bioorganic Chemistry and Molecular Engineering of Ministry of Education, PKU-IDG/McGovern Institute for Brain Research, Peking University, Beijing 100871, China; Academy for Advanced Interdisciplinary Studies, Peking-Tsinghua Center for Life Sciences and Beijing Advanced Center of RNA Biology (BEACON), Peking University, Beijing 100871, China; Chinese Institute for Brain Research (CIBR), Beijing 102206, China;* orcid.org/0000-0002-9798-5242; Email: zoupeng@pku.edu.cn

Authors

Tianyu Ren − *State Key Laboratory of Chemo/Biosensing and Chemometrics, College of Chemistry and Chemical Engineering, Hunan University, Changsha 410082, China*

Jinsaibo Gong − *College of Chemistry and Molecular Engineering, Synthetic and Functional Biomolecules Center, Beijing National Laboratory for Molecular Sciences, Key*

https://doi.org/10.1021/acs.analchem.5c01826
Anal. Chem. 2025, 97, 14492−14502

Laboratory of Bioorganic Chemistry and Molecular Engineering of Ministry of Education, PKU-IDG/McGovern Institute for Brain Research, Peking University, Beijing 100871, China

Fu Zheng − *College of Chemistry and Molecular Engineering, Synthetic and Functional Biomolecules Center, Beijing National Laboratory for Molecular Sciences, Key Laboratory of Bioorganic Chemistry and Molecular Engineering of Ministry of Education, PKU-IDG/McGovern Institute for Brain Research, Peking University, Beijing 100871, China*

Jinshan Long − *State Key Laboratory of Chemo/Biosensing and Chemometrics, College of Chemistry and Chemical Engineering, Hunan University, Changsha 410082, China*

Han Wang − *College of Chemistry and Molecular Engineering, Synthetic and Functional Biomolecules Center, Beijing National Laboratory for Molecular Sciences, Key Laboratory of Bioorganic Chemistry and Molecular Engineering of Ministry of Education, PKU-IDG/McGovern Institute for Brain Research, Peking University, Beijing 100871, China*

Complete contact information is available at: https://pubs.acs.org/10.1021/acs.analchem.5c01826

Author Contributions

#T.R. and J.G. contributed equally to this work. J.H. and P.Z. conceived the project and designed the experiments; T.R. performed chemical synthesis and characterization; J.G. and F.Z. performed cellular labeling and proteomics experiments; T.R., J.G., F.Z., J.H., and P.Z. analyzed the data; J.G., T.R., J.H., and P.Z. wrote the paper with input from all authors. All authors have given approval to the final version of the manuscript.

Notes

The authors declare no competing financial interest.

■ ACKNOWLEDGMENTS

This work was supported by the Ministry of Science and Technology (2022YFA1304700), the National Natural Science Foundation of China (32088101, 22204046), and Beijing National Laboratory for Molecular Sciences (BNLMS-CXXM-202403). The measurements of Mass Spectrometry were performed at the Analytical Instrumentation Center of Peking University. The help from PKUAIC (Dr. Wen Zhou) is acknowledged.

■ REFERENCES

(1) Zhou, Y.; Zou, P. *Curr. Opin. Chem. Biol.* **2021**, *60*, 30−38.
(2) Verdin, E.; Hirschey, M. D.; Finley, L. W.; Haigis, M. C. *Trends Biochem. Sci.* **2010**, *35* (12), 669−675.
(3) Kilbride, S. M.; Prehn, J. H. *Oncogene* **2013**, *32* (22), 2703−2711.
(4) Wei, W.; Riley, N. M.; Yang, A. C.; Kim, J. T.; Terrell, S. M.; Li, V. L.; Garcia-Contreras, M.; Bertozzi, C. R.; Long, J. Z. *Nat. Chem. Biol.* **2021**, *17* (3), 326−334.
(5) Huh, W.-K.; Falvo, J. V.; Gerke, L. C.; Carroll, A. S.; Howson, R. W.; Weissman, J. S.; O'Shea, E. K. *Nature* **2003**, *425* (6959), 686−691.
(6) Rhee, H.-W.; Zou, P.; Udeshi, N. D.; Martell, J. D.; Mootha, V. K.; Carr, S. A.; Ting, A. Y. *Science* **2013**, *339* (6125), 1328−1331.
(7) Lam, S. S.; Martell, J. D.; Kamer, K. J.; Deerinck, T. J.; Ellisman, M. H.; Mootha, V. K.; Ting, A. Y. *Nat. Methods* **2015**, *12* (1), 51−54.
(8) Loh, K. H.; Stawski, P. S.; Draycott, A. S.; Udeshi, N. D.; Lehrman, E. K.; Wilton, D. K.; Svinkina, T.; Deerinck, T. J.; Ellisman, M. H.; Stevens, B.; et al. *Cell* **2016**, *166* (5), 1295−1307.e21.
(9) Roux, K. J.; Kim, D. I.; Raida, M.; Burke, B. *J. Cell Biol.* **2012**, *196* (6), 801−810.
(10) Branon, T. C.; Bosch, J. A.; Sanchez, A. D.; Udeshi, N. D.; Svinkina, T.; Carr, S. A.; Feldman, J. L.; Perrimon, N.; Ting, A. Y. *Nat. Biotechnol.* **2018**, *36* (9), 880−887.
(11) Qin, W.; Cho, K. F.; Cavanagh, P. E.; Ting, A. Y. *Nat. Methods* **2021**, *18* (2), 133−143.
(12) Zhang, B.; Zhang, Y.; Liu, J.-L.; Andrews, B. J. *G3* **2021**, *11* (5), jkab077.
(13) Kim, K.-e.; Park, I.; Kim, J.; Kang, M.-G.; Choi, W. G.; Shin, H.; Kim, J.-S.; Rhee, H.-W.; Suh, J. M. *Nat. Commun.* **2021**, *12* (1), 5204.
(14) Sun, X.; Sun, H.; Han, X.; Chen, P. C.; Jiao, Y.; Wu, Z.; Zhang, X.; Wang, Z.; Niu, M.; Yu, K.; Liu, D.; Dey, K. K.; Mancieri, A.; Fu, Y.; Cho, J. H.; Li, Y.; Poudel, S.; Branon, T. C.; Ting, A. Y.; Peng, J. *Anal. Chem.* **2022**, *94* (13), 5325−5334.
(15) Takano, T.; Wallace, J. T.; Baldwin, K. T.; Purkey, A. M.; Uezu, A.; Courtland, J. L.; Soderblom, E. J.; Shimogori, T.; Maness, P. F.; Eroglu, C.; Soderling, S. H. *Nature* **2020**, *588* (7837), 296−302.
(16) Rayaprolu, S.; Bitarafan, S.; Santiago, J. V.; Betarbet, R.; Sunna, S.; Cheng, L.; Xiao, H.; Nelson, R. S.; Kumar, P.; Bagchi, P.; et al. *Nat. Commun.* **2022**, *13* (1), 2927.
(17) Liu, Y.; Zeng, R.; Wang, R.; Weng, Y.; Wang, R.; Zou, P.; Chen, P. R. *Proc. Natl. Acad. Sci. U. S. A.* **2021**, *118* (25), No. e2025299118.
(18) Lee, S. Y.; Cheah, J. S.; Zhao, B.; Xu, C.; Roh, H.; Kim, C. K.; Cho, K. F.; Udeshi, N. D.; Carr, S. A.; Ting, A. Y. *Nat. Methods* **2023**, *20* (6), 908−917.
(19) Qu, D.; Li, Y.; Liu, Q.; Cao, B.; Cao, M.; Lin, X.; Shen, C.; Zou, P.; Zhou, H.; Zhang, W.; Pan, W. *Cell Res.* **2025**, *35*, 149−152.
(20) Toh, K.; Nishio, K.; Nakagawa, R.; Egoshi, S.; Abo, M.; Perron, A.; Sato, S. I.; Okumura, N.; Koizumi, N.; Dodo, K.; Sodeoka, M.; Uesugi, M. *J. Am. Chem. Soc.* **2022**, *144* (44), 20171−20176.
(21) Geri, J. B.; Oakley, J. V.; Reyes-Robles, T.; Wang, T.; McCarver, S. J.; White, C. H.; Rodriguez-Rivera, F. P.; Parker, D. L.; Hett, E. C.; Fadeyi, O. O.; Oslund, R. C.; MacMillan, D. W. C. *Science* **2020**, *367* (6482), 1091−1097.
(22) Buksh, B. F.; Knutson, S. D.; Oakley, J. V.; Bissonnette, N. B.; Oblinsky, D. G.; Schwoerer, M. P.; Seath, C. P.; Geri, J. B.; Rodriguez-Rivera, F. P.; Parker, D. L.; Scholes, G. D.; Ploss, A.; MacMillan, D. W. *J. Am. Chem. Soc.* **2022**, *144* (14), 6154−6162.
(23) Muller, M.; Grabnitz, F.; Barandun, N.; Shen, Y.; Wendt, F.; Steiner, S. N.; Severin, Y.; Vetterli, S. U.; Mondal, M.; Prudent, J. R.; et al. *Nat. Commun.* **2021**, *12* (1), 7036.
(24) Tay, N. E. S.; Ryu, K. A.; Weber, J. L.; Olow, A. K.; Cabanero, D. C.; Reichman, D. R.; Oslund, R. C.; Fadeyi, O. O.; Rovis, T. *Nat. Chem.* **2023**, *15* (1), 101−109.
(25) Takato, M.; Sakamoto, S.; Nonaka, H.; Tanimura Valor, F. Y.; Tamura, T.; Hamachi, I. *Nat. Chem. Biol.* **2025**, *21* (1), 109−119.
(26) Wang, P.; Tang, W.; Li, Z.; Zou, Z.; Zhou, Y.; Li, R.; Xiong, T.; Wang, J.; Zou, P. *Nat. Chem. Biol.* **2019**, *15* (11), 1110−1119.
(27) Hananya, N.; Ye, X.; Koren, S.; Muir, T. W. *Proc. Natl. Acad. Sci. U. S. A.* **2023**, *120* (16), No. e2219339120.
(28) Zheng, F.; Yu, C.; Zhou, X.; Zou, P. *Nat. Commun.* **2023**, *14* (1), 2978.
(29) Zhai, Y.; Huang, X.; Zhang, K.; Huang, Y.; Jiang, Y.; Cui, J.; Zhang, Z.; Chiu, C. K. C.; Zhong, W.; Li, G. *Nat. Commun.* **2022**, *13* (1), 4906.
(30) Tong, F.; Zhou, W.; Janiszewska, M.; Seath, C. P. *J. Am. Chem. Soc.* **2025**, *147* (11), 9316−9327.
(31) Haag, S. M.; Gulen, M. F.; Reymond, L.; Gibelin, A.; Abrami, L.; Decout, A.; Heymann, M.; van der Goot, F. G.; Turcatti, G.; Behrendt, R.; Ablasser, A. *Nature* **2018**, *559* (7713), 269−273.
(32) Wang, Y.; Wen, X.; Zhang, N.; Wang, L.; Hao, D.; Jiang, X.; He, G. *Biomed. Pharmacother.* **2019**, *118*, 109203.
(33) Du, X.; Huang, S.; Lin, Z.; Chen, G.; Jiang, Y.; Zhang, H. *Chem. Commun.* **2025**, *61* (40), 7236−7252.
(34) Los, G. V.; Encell, L. P.; McDougall, M. G.; Hartzell, D. D.; Karassina, N.; Zimprich, C.; Wood, M. G.; Learish, R.; Ohana, R. F.; Urh, M.; Simpson, D.; Mendez, J.; Zimmerman, K.; Otto, P.;

Vidugiris, G.; Zhu, J.; Darzins, A.; Klaubert, D. H.; Bulleit, R. F.; Wood, K. V. *ACS Chem. Biol.* **2008**, *3* (6), 373−382.
(35) Kompa, J.; Bruins, J.; Glogger, M.; Wilhelm, J.; Frei, M. S.; Tarnawski, M.; D'Este, E.; Heilemann, M.; Hiblot, J.; Johnsson, K. *J. Am. Chem. Soc.* **2023**, *145* (5), 3075−3083.
(36) Bottone, S.; Joliot, O.; Cakil, Z. V.; El Hajji, L.; Rakotoarison, L. M.; Boncompain, G.; Perez, F.; Gautier, A. *Nat. Methods* **2023**, *20* (10), 1553−1562.
(37) He, J.; Wang, Y.; Missinato, M. A.; Onuoha, E.; Perkins, L. A.; Watkins, S. C.; St Croix, C. M.; Tsang, M.; Bruchez, M. P. *Nat. Methods* **2016**, *13* (3), 263−268.
(38) Telmer, C. A.; Verma, R.; Teng, H.; Andreko, S.; Law, L.; Bruchez, M. P. *ACS Chem. Biol.* **2015**, *10* (5), 1239−1246.
(39) Li, L.; Han, J.; Lo, H. G.; Tam, W. W. L.; Jia, H.; Tse, E. C. M.; Taliaferro, J. M.; Li, Y. *Nucleic Acids Res.* **2024**, *52* (7), No. e36.
(40) Deng, Z.; Li, L.; Jia, H.; Li, N.-F.; He, J.; Li, M.-D.; Phillips, D. L.; Li, Y. *Chem. - Eur. J.* **2023**, *29* (16), No. e202203684.
(41) Wang, Y.; Ballou, B.; Schmidt, B. F.; Andreko, S.; St Croix, C. M.; Watkins, S. C.; Bruchez, M. P. *Chem. Commun.* **2017**, *53* (12), 2001−2004.
(42) Zhai, Y.; Zhang, X.; Chen, Z.; Yan, D.; Zhu, L.; Zhang, Z.; Wang, X.; Tian, K.; Huang, Y.; Yang, X.; Sun, W.; Wang, D.; Tsai, Y. H.; Luo, T.; Li, G. *Nat. Chem.* **2024**, *16* (9), 1546−1557.
(43) Lu, P.; Liu, X.; Chu, X.; Wang, F.; Jiang, J. H. *Chem. Sci.* **2023**, *14* (10), 2562−2571.
(44) Rath, S.; Sharma, R.; Gupta, R.; Ast, T.; Chan, C.; Durham, T. J.; Goodman, R. P.; Grabarek, Z.; Haas, M. E.; Hung, W. H. W.; Joshi, P. R.; Jourdain, A. A.; Kim, S. H.; Kotrys, A. V.; Lam, S. S.; McCoy, J. G.; Meisel, J. D.; Miranda, M.; Panda, A.; Patgiri, A.; Rogers, R.; Sadre, S.; Shah, H.; Skinner, O. S.; To, T. L.; Walker, M. A.; Wang, H.; Ward, P. S.; Wengrod, J.; Yuan, C. C.; Calvo, S. E.; Mootha, V. K. *Nucleic Acids Res.* **2021**, *49* (D1), D1541−D1547.
(45) Thul, P. J.; Akesson, L.; Wiking, M.; Mahdessian, D.; Geladaki, A.; Ait Blal, H.; Alm, T.; Asplund, A.; Bjork, L.; Breckels, L. M.; et al. *Science* **2017**, *356* (6340), No. eaal3321.

https://doi.org/10.1021/acs.analchem.5c01826
Anal. Chem. 2025, 97, 14492−14502